

# Local and remote response of the North Sea dynamics to morphodynamic changes in the Wadden Sea

Benjamin Jacob<sup>1</sup> · Emil Vassilev Stanev<sup>2</sup> · Yinglong Joseph Zhang<sup>3</sup>

Received: 14 July 2015 / Accepted: 15 March 2016 / Published online: 31 March 2016  
© Springer-Verlag Berlin Heidelberg 2016

**Abstract** The response of the tidal system in the southern North Sea to morphodynamic changes was investigated in a modelling study using fine resolution bathymetric observations available for 1982–2011. The Semi-implicit Cross-scale Hydrosience Integrated System Model (SCHISM) was set up for the different sets of bathymetries. One set of bathymetry was compiled from a large number of bathymetric measurements over many years, while the other two reflected bathymetry state in the area of Wadden Sea during 2000 and 2011, respectively. The temporal and spatial evolution of bathymetry was dominated by migration of tidal channels. The M4 tide showed larger sensitivity to bathymetric change in the Wadden Sea than the M2 tide, whereas the structure of the latter remained rather robust. The largest change of the tidal wave due to the differences in bathymetries was located off the North Frisian Wadden Sea. Traces of changes were also found far away from the regions of

their origin because the tidal waves in the North Sea propagate the local disturbances basin-wide. This illustrated an efficient physical mechanism of teleconnectivity, i.e. effecting the local responses to the larger-scale or remote change of ocean bottom caused by erosion and deposition. The tidal distortion resulting from the relatively small bathymetric changes was substantial, particularly in the coastal zone. This is a manifestation of the nonlinear tidal transformation in shallow oceans and is crucial for the sediment transport and the morphodynamic feedback, because of the altered tidal asymmetry.

**Keywords** Bathymetry · Sensitivity study · North Sea · Tides

## 1 Introduction

While most of the input of mechanical energy into the ocean due to the tide generating forces occurs in the open oceans, it is inside the coastal ocean where the largest amount of this energy is dissipated. The shallow water bathymetry is a key factor controlling the dissipation. Coupled hydrodynamics and sediment dynamics in the shallow ocean are important drivers of bathymetric changes there. For these areas, bathymetry is no longer constant in time; however, the limited amount of consistent and synoptic data over larger areas makes it difficult to estimate the rates of morphodynamic changes and the resulting hydrodynamic response.

The motivation for the present study originates from the recent analysis of bathymetric changes in the Wadden Sea described by Winter (2011), who analysed the morphological evolution along the German North Sea coast and quantified the bed elevation range from echo sounding measurements. He demonstrated that the highest morphological

---

Responsible Editor: Han Winterwerp

---

✉ Benjamin Jacob  
benjamin.jacob@uni-oldenburg.de

Emil Vassilev Stanev  
emil.stanev@hzg.de

<sup>1</sup> Institute for Biology and Chemistry of the Marine Environment, University of Oldenburg, Oldenburg, Lower-Saxony, Germany

<sup>2</sup> Institute for Coastal Research, University of Oldenburg, Helmholtz-Zentrum Geesthacht, Schleswig-Holstein, Germany

<sup>3</sup> Center for Coastal Resources Management, College of William & Mary, Virginia Institute of Marine Science, Gloucester Point, VA 23062, USA

activity can be found in the vicinity of tidal channels. What is still unknown is the local and remote impact of these morphodynamic changes. This is the main research question addressed in the present study. This question is not a trivial one because the large-scale effects due to small-scale topographic changes are still unclear and their detection from observations is not easy.

The overall role of bottom bathymetry for the ocean circulation has been addressed in a number of numerical modelling studies in the twentieth century. In the past decades, further understanding of the impact of ocean bottom morphology on tides and associated processes has been attained (Le Provost et al. 2003). It has been recognised that the uncertainties in bathymetric data present a major problem when modelling the processes controlled by long surface gravity waves (tides, storm surges, tsunamis, and seiches). These processes, which are associated with strong local currents of shorter temporal and spatial scales, depend strongly on shallow water bathymetry, coastal shoreline, and underwater channels over continental shelves.

Fine resolution numerical models need fine resolution bathymetric maps (e.g. GEBCO data IOC, IHO and BODC 2003 or finer ones in the coastal ocean). However, the actual improvement of fine-resolution maps is strongly dependent on the available bathymetric observations, which in most cases are not sufficient. Therefore, different kind of observations can be used to constrain estimation of bottom bathymetry (see Zaron et al. 2011, who provided an excellent and concise overview). Heemink et al. (2002) used observed water level to adjust values of bottom depth and roughness coefficient.

Adjoint-based methods were used by Losch and Wunsch (2003) to identify large-scale bottom bathymetry from sea surface height data. Sea level model error statistics due to uncertainties in bathymetry in shallow seas were addressed by Mourre et al. (2004). In the study of Hirose (2005), bathymetric datasets were compared and assessed with constraints from an ocean current model and velocity observations. The above-cited studies demonstrated that the coastal prediction capabilities are limited by a lack of accurate bathymetric data (see also Ezer and Liu 2010) and advocated for advanced use of data assimilation approaches in the field of coastal morphodynamics (e.g. Scott and Mason 2007; Smith et al. 2009; Garcia et al. 2013).

So far, little is known about the effect of small-scale coastal morphological features on the tidal system. In order to investigate this issue, we use high-resolution bathymetric data and numerical simulations with an unstructured-grid model (SCHISM, Zhang et al. 2015b) for the southern North Sea. SCHISM stands for Semi-implicit Cross-scale Hydroscience Integrated System Model.

In the present study, we do not address the full complexity of effects governing the morphodynamic evolution of

coastal systems or all possible responses in the North Sea. The second issue is addressed in more detail by Schulz-Stellenfleth and Stanev (2015) who studied the impact of small scale perturbations of bathymetry, bottom roughness, wind forcing and boundary forcing. They used a relatively simpler (two-dimensional linear barotropic) model solved in the spectral domain and estimated the impact of different types of perturbations by inversion of the model. Different from the study of Schulz-Stellenfleth and Stanev (2015), we use realistic bathymetries and an up-to-date numerical model, which is capable of resolving small-scale processes in the coastal zone.

The results presented here address one fundamental problem of oceanography, namely how important it is to use time-referenced bathymetric data accounting for temporal and spatial variability of ocean bottom. Thus, the challenging question is: can we have adequate coastal and estuarine predictions if bottom maps do not correspond to the current state of morphodynamic systems. Another fundamental question is how much the tidal response is dependent on the migration of underwater channels. This migration, which can be considered as change in the macro bottom roughness, could impact larger ocean areas.

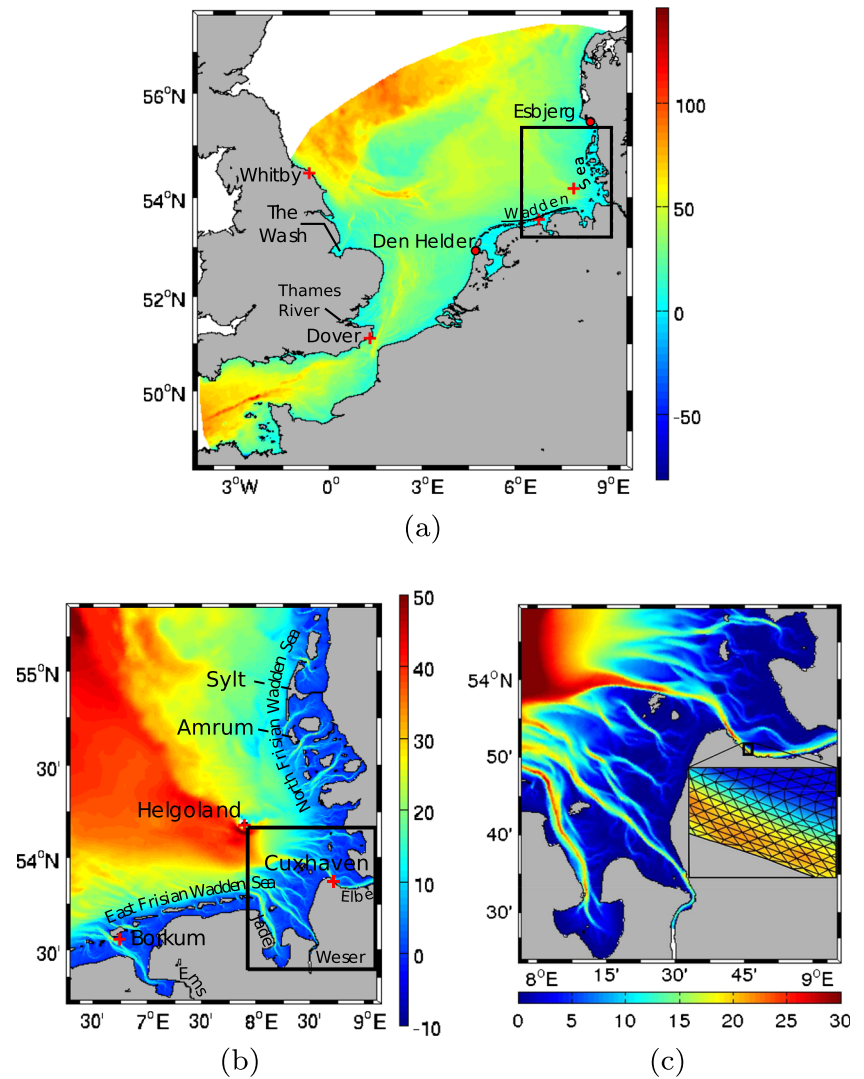
The paper is structured as follows. In Section 2, we describe the study area and its variability. In Section 3, we describe the numerical model, its performance and validation. Results of sensitivity experiments are presented in Section 4, followed by discussion in Section 5 and short conclusions in Section 6.

## 2 The study area

### 2.1 General characteristics

We address in this study the southern North Sea (Fig. 1a) which is a flat shelf sea. Because the extent of the North Sea is small, it cannot locally produce a significant response to the astronomical tides, but is mostly driven by the tidal currents from its northern boundary and English Channel. The tidal wave (Kelvin wave) travels in a counter clock-wise direction; the major tidal constituent is the lunar semi-diurnal tide. The Wadden Sea, which is in the south eastern corner of the German Bight (Fig. 1b) and is the shallowest part of North Sea, is a meso-tidal area stretching from Den Helder in the Netherlands to Esbjerg in Denmark. It is characterised by complex dynamics, caused by a variety of topographic features such as barrier islands, tidal inlets, ebb/flood deltas, tidal flats and tidal channels. Tidal flats are subject to periodic wetting and drying. They are intersected by a network of deep tidal channels (Fig. 1c), which works as a flooding and drainage system that channelises the

**Fig. 1** Bathymetry (in m) derived from the digital elevation map used in the reference run (BR) shown for (a) the southern North Sea (the model domain) and zooms to (b) the German Bight and (c) part of Wadden Sea (c) giving more detail about the small-scale topographic features. The inset in (c) represents part of the model grid illustrating that bathymetric channels are sufficiently resolved in the numerical model. The tide gauge stations used for model validation are marked (+). White areas are ocean areas, which are outside the model grid. The same conventions applies to other similar figures



flow during flood and ebb period. The mixing between the freshwater and seawater creates complex stratification, vertical circulation and two-way exchange in the tidal channels.

Of utmost importance for the present study is the fact that the bathymetry of the Wadden Sea is continuously reshaped by the transport of sediments due to currents and waves, resulting in a pronounced morphodynamic change (Winter 2011). In these areas, the nonlinear tidal distortion, which is characterised by complex patterns of generation of overtides (Stanev et al. 2014), results in a complex asymmetric deformation of tides. This asymmetry largely controls the sediment transport (Stanev et al. 2006; Robins and Davies 2010). Multiple feedback mechanisms affect the growth of instabilities associated with morphological changes, driving the current coastal-ocean state towards new operational modes (e.g. the infilling of deep estuaries with marine sediments or the migration of tidal channels); however, the dynamic effects of these changes are not well understood.

## 2.2 Observed changes in bathymetry

### 2.2.1 Macro bottom roughnesses

The recent study of Schulz-Stellenfleth and Stanev (2015) addressed the impact of small-scale perturbations of bathymetry on the dynamics of North Sea, demonstrating that the German Bight area stands out in its sensitivity. However, this theoretical study addressed 2D linear barotropic tides; perturbations were represented as white noise. Because in the present study we are interested in the impact of realistic bathymetry changes, we discuss in the following the evolution of bathymetry in the German Bight from 1982 to 2011.

The first digital elevation model (DEM), which we will refer to as bathymetry reference (BR), uses the bathymetric data compiled from a large number of bathymetric measurements provided by the Bundesamt für Seeschifffahrt und Hydrographie (BSH). Therefore, BR is a hypothetical DEM

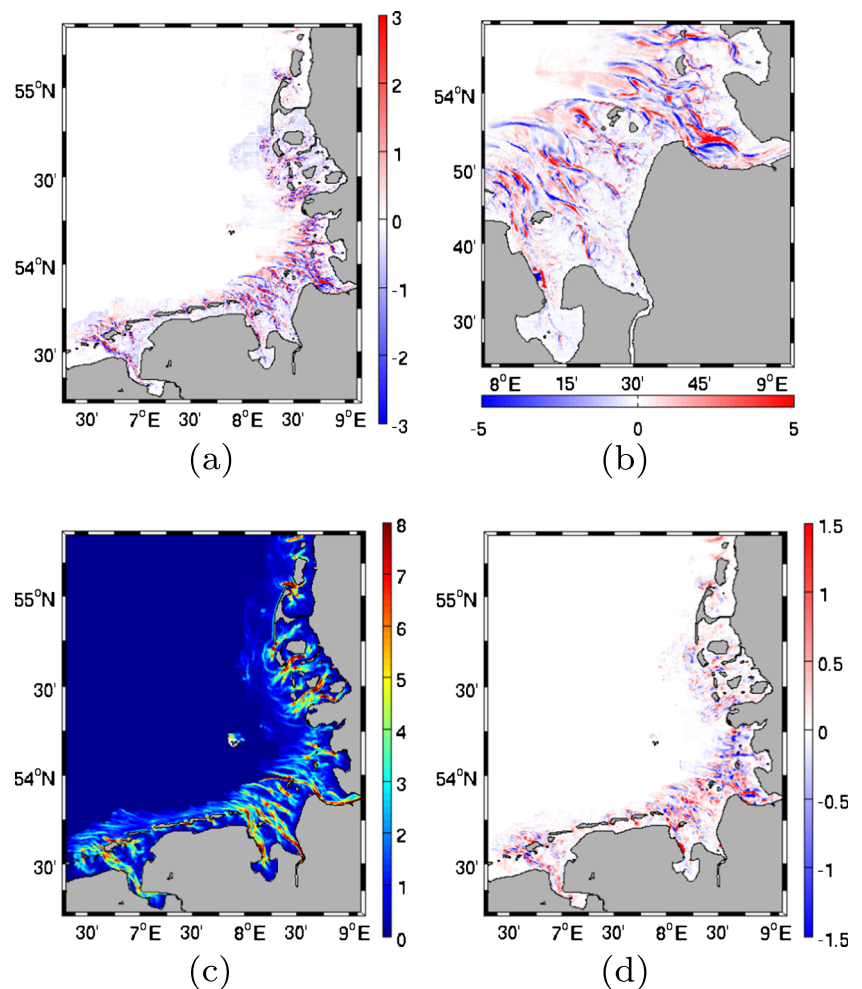
reflecting the mean conditions rather than corresponding to a particular time. Mapping onto model grid was done at the Helmholtz-Zentrum Geesthacht. As demonstrated in Fig. 1, this bathymetry resolves well both the large scale and small-scale topographic elements.

The second and third DEMs were derived from the first DEM by merging it with data from the bathymetry products of the German Coastal Engineering Research Council project AufMod (Aufbau integrierter Modellsysteme zur Analyse der langfristigen Morphodynamik in der Deutschen Bucht) for the years 2000 and 2011, respectively. These two data sets are quasi-synoptic bathymetric time slices, which will be referred to as time-referenced data sets. Their spatial extent is the German Bight from the coast towards the 20 m isobath (for more information see, e.g. Heyer and Schrottko 2013). Thus, the resulting DEMs are different from BR only within the extent of the Aufmod data (the German Wadden Sea), but identical elsewhere. The coast in the two topographies is the same because dikes are fixed. The new time-referenced DEMs hereafter will be referred to as B2000 and B2011.

The difference map (B2011–B2000) in Fig. 2a shows alternating patterns caused by deposition (negative depth differences) and erosion (positive depth differences). The zoom-in around the south eastern coast (Fig. 2b) reveals the change in the channel structure between the two topographies. The migration of tidal channels (the positive deviations represent the former route of the channel, and the negative ones represent the new route of the channel) reaches vertical amplitudes of about 5 m. The magnitude of bathymetric changes decreases in the open sea.

Some authors define surface roughness in terms of the variability of elevation values, generally expressed as the absolute standard deviation of all values within a window or as the deviation from a best-fit plane (Grohmann et al. 2009). In our case, the standard deviation of depth around a radius of 1 km computed from B2011 (Fig. 2c) gives an overall idea about the patterns of macro bottom roughness, which describes the structural heterogeneity of the bathymetry and reveals the small-scale bottom features. Since patterns in macro roughness are linked to the location of tidal channels, the difference between macro bottom

**Fig. 2** Morphodynamic changes represented by the difference (in m) between the bathymetries for the year 2000 (B2000) and 2011 (B2011) in the German Bight (**a**) and in its south-eastern corner (**b**). **c** shows the macro roughness elements represented by the standard deviation of depth (in m) around a radius of 1 km in B2011. **d** shows the difference between macro roughnesses in B2000 and B2011 (in m). Differences are positive if values of B2011 exceed those of B2000





roughnesses in B2011 and B2000 (Fig. 2) shows alternating patterns of increased and decreased macro roughness, which are qualitatively similar to the major depth changes (Fig. 2a,b). Hence, positive and negative changes in roughness, which are mostly related to the migration of channels, are more or less balanced, although positive deviations seem dominant in some regions, such as the inlets in the northmost of Fig. 2d.

### 2.2.2 Migration of tidal channels

Large differences between bathymetries observed in individual years motivate the analysis on temporal variability and its regional characteristics. Results of previous section justify focusing on the corner of German Bight where the variance of topography estimated for the period 1982–2011 is largest.

The location of these maxima (Fig. 3a (“continuous bathymetry” is only available where the standard deviation is non zero)) demonstrates that largest morphodynamic changes occur in the regions of tidal channels (Winter 2011).

Bottom anomaly, defined as the difference between current and mean depth for the period 1982–2011 along the

section line in Fig. 3a, demonstrates that morphodynamic change in Jade Channel is relatively small. Variations in the area of Weser Channel at about 20 km are characterised by recurrent positive and negative changes with recurrent time of about 20 years. Largest are the changes in the area of Elbe Channel (around 60 km) where there are some indications of eastward propagating disturbances as estimated from the slopes of positive and negative contours. Theoretically, one would expect that these morphological changes could affect propagation of tidal waves and other regional processes.

### 2.3 Seasonal-to-interannual variability as seen in tide gauge data

It is well-known that tidal signals undergo substantial distortion in coastal zone. This can be understood as a nonlinear growth of harmonics of the principal tides (Dronkers 1964; Pingree and Griffiths 1979). Nonlinear advection terms are responsible for the generation of even harmonic overtides, for instance M4; nonlinear friction is responsible for producing odd harmonic overtides such as M6 (Friedrichs and Aubrey 1988; Speer and Aubrey 1985; Parker 1991). These effects are quite pronounced also in the German Bight (Dronkers 1986; Stanev et al. 2014).

Long-term sea level measurements (e.g. from tidal gauges) can be used to check whether shifts in tidal signals or pronounced variabilities exist and/or can be related to possible drivers. Typical drivers are changes in the climatological boundary conditions such as mean sea level rise and air pressure. However, vertical movement of land masses (glacio iso-static adjustment) or changes associated with geomorphological processes or human interventions (e.g. dikes and dredging) could also result in sea-revel responses, especially in the coastal zone, where water is shallow and changes in depth become comparable to its mean value. In most of the above-mentioned cases, changes in depth affect the propagation speed of the barotropic tide ( $\sqrt{gH}$ ). Besides depth the bottom roughness associated with migration of dunes and channels can also affect barotropic tide.

Mudersbach et al. (2013) used observations throughout the twentieth century and early twenty-first century to demonstrate that sea level in the German Bight during 1950s to 1990s showed significantly different variability from the mean sea level. They attributed this to changes in the amplitudes of several main tidal constituents and decadal variability in the storm activity. Gräwe et al. (2014) reported on the variability of tidal constituents (of 8–10 % for M2 and 12–30 % for M4), with larger amplitudes in summer than in winter. This variability was explained as a result of changing stratification (e.g. summer thermocline), which can affect the internal friction in the water column and thus bottom friction, and the latter is very important for the propagation of barotropic tide (Müller 2012). Similar responses

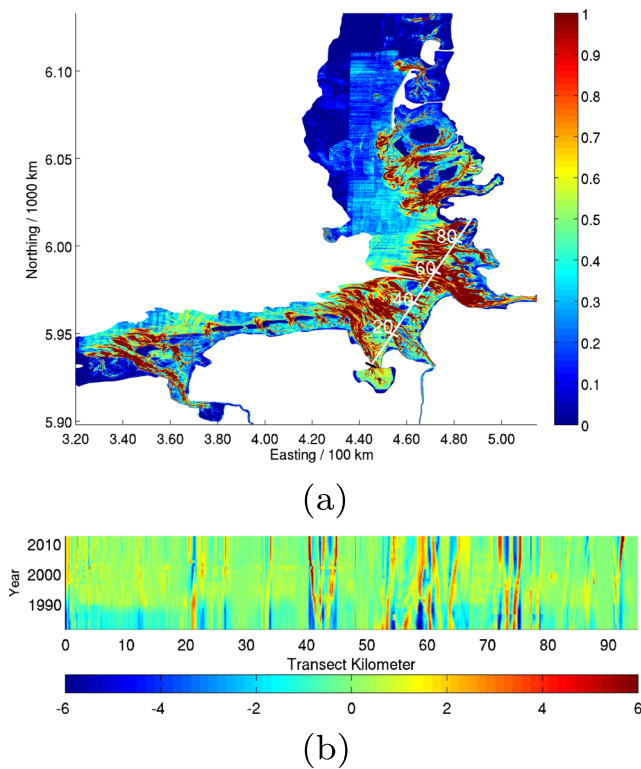


**Fig. 3** Migration of tidal channels. **a** standard deviation of topography (in m) computed from the 30 bathymetric maps (1982–2011) from AufMod. **White line** is a transect along which morphodynamic changes in **(b)** are analysed. Numbers on this line identify positions to which references are given in text

to thermohaline changes can be even more important in the estuarine domains, where variability of river flows and strong salinity gradients in the coastal ocean can couple with barotropic tides.

One would expect that changes in bathymetry reported in the previous section could trigger changes in tidal composition and enhance the feedback between hydrodynamics and morphodynamics. If this was the case, one could expect certain coherence between changes in bathymetry and tides recorded in gauge stations. Led by this argument, we will analyse in the following the tidal composition in the southern North Sea with a focus on M2 and M4 tide. Their ratio can be instructive for tidal asymmetry which controls the sediment transport.

Tidal gauge data in the last decades at several coastal stations, which were kindly provided by the German Maritime and Hydrographic Agency and Wasser- und Schifffahrtsverwaltung des Bundes (WSV) via the Bundesanstalt für Gewässerkunde, BfG are analysed with a focus on inter-annual and seasonal variability of tidal constituents. The results in Fig. 4 reveal a clear seasonal cycle of M2 tide in Cuxhaven with maximum amplitudes in summer and minimum amplitudes in autumn supporting the analysis of Gräwe et al. (2014). The variability of M4 tide is much less regular (Fig. 4b). The relative change of M4 amplitude is about two times larger than the one of M2 tide at Helgoland. At Borkum station, this factor is about four. As far as the ratio between amplitudes of M2 and M4 tides is concerned, Fig. 4c shows large variations. Regional variations of this ratio estimated at the individual coastal stations also vary greatly. It appears difficult to derive from available

data clear statements about interannual variability of tidal constituents and asymmetry of tidal signal, which could be related to the morphodynamic changes reported above. Therefore, a theoretical study could help to at least investigate the ranges of response induced by bottom change.

### 3 The numerical model

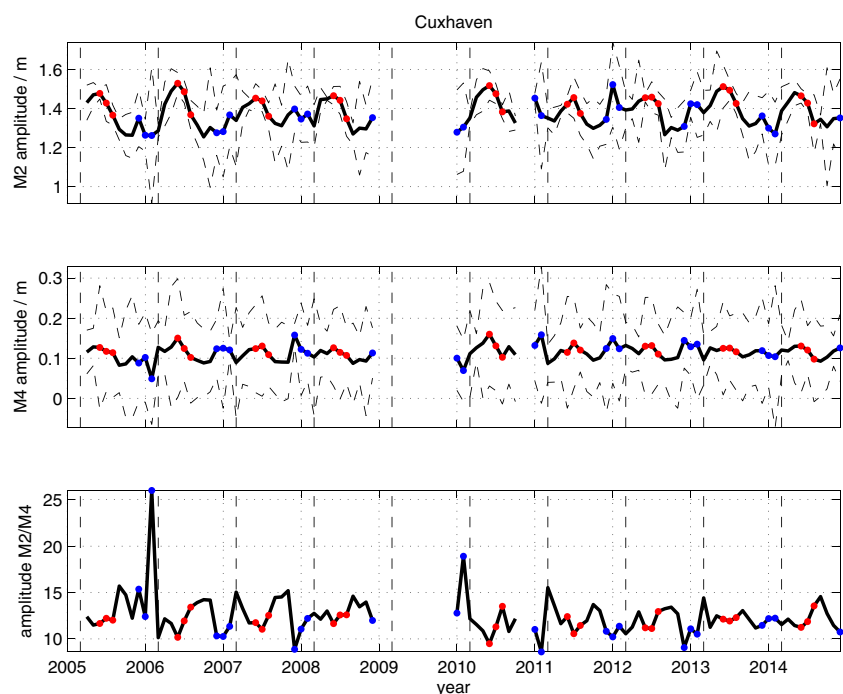
#### 3.1 Description of the numerical model

##### 3.1.1 The model equations of SCHISM

In order to simulate the dynamics of the southern North Sea, we use SCHISM (Zhang et al. 2015b), which was derived from SELFE (Zhang and Baptista 2008). SCHISM is a 3D model using Boussinesq and hydrostatic approximations to solve the continuity, momentum and transport equations for salt and heat. Under these assumptions and with the following notation:

- $(x, y) :=$  horizontal Cartesian coordinates (m);
- $z :=$  vertical coordinate (positive upward with the undisturbed sea surface as reference level) (m);
- $\nabla := \left( \frac{\partial}{\partial x}, \frac{\partial}{\partial y} \right);$
- $t :=$  time (s);
- $\eta(x, y, t) :=$  free-surface elevation (m);
- $h(x, y) :=$  bathymetric depth (m);
- $\mathbf{u}(x, y, z, t) :=$  horizontal velocity, with Cartesian components  $(u, v)$  ( $\text{m s}^{-1}$ );
- $w :=$  vertical velocity ( $\text{m s}^{-1}$ );

**Fig. 4** Monthly amplitude of tidal constituents (—) for **a** M2, **b** M4 and **c** the ratio M2/M4, calculated from sea level measurements at tide gauge station Cuxhaven. Dots highlight summer (JJA: ●) and winter (NDJ: ●) month within an atmospheric year (Feb-Jan: indicated by vertical dashed lines). In **(a)** and **(b)** the error range of the harmonic analysis is given as 95 % confidence interval (---)



- $f$  := Coriolis factor ( $s^{-1}$ );
- $g$  := acceleration of gravity ( $m\ s^{-2}$ );
- $\psi_e(\phi, \lambda)$  := earth-tidal potential (m) at latitude ( $\phi$ ) and longitude ( $\lambda$ );
- $\alpha$  := effective earth-elasticity factor ( $= 0.69$ );
- $\rho(\mathbf{x}, t)$  := water density, with a reference value of  $\rho_0 = 1025\ kg\ m^{-3}$  (Boussinesq approximation);
- $p_A(x, y, t)$  := atmospheric pressure at the free surface ( $N\ m^{-2}$ );
- $v$  := vertical eddy viscosity ( $m^2\ s^{-1}$ );
- $\mu$  := horizontal eddy viscosity ( $m^2\ s^{-1}$ );
- $S, T$  := salinity, temperature of the water (practical salinity units (psu),  $^{\circ}C$ );
- $\kappa$  := vertical eddy diffusivity, for salt and heat ( $m^2\ s^{-1}$ );
- $F_s, F_h$  := horizontal diffusion for transport equations (in SCHISM using default values of zero and operating with the numerical diffusivity);
- $\dot{Q}$  := rate of absorption of solar radiation ( $m^{-2}$ );
- $C_p$  := specific heat of water ( $J\ kg^{-1}\ K^{-1}$ ).

the governing 3D equations in Cartesian coordinates write

$$\nabla \cdot \mathbf{u} + \frac{\partial w}{\partial z} = 0 \tag{1}$$

for the continuity equation and

$$\frac{\partial \eta}{\partial t} + \nabla \cdot \int_{-h}^{\eta} \mathbf{u} dz = 0 \tag{2}$$

for the equation of free surface elevation. Applying the Boussinesq approximation the horizontal momentum equation is given by

$$\begin{aligned} \frac{d\mathbf{u}}{dt} &= \mathbf{f} - g\nabla\eta + \frac{\partial}{\partial z} \left( v \frac{\partial \mathbf{u}}{\partial z} \right) - \frac{1}{\rho_0} \nabla p_A - \frac{g}{\rho_0} \int_z^{\eta} \nabla \rho d\zeta \\ &+ \nabla \cdot (\mu \nabla \mathbf{u}), \\ \mathbf{f} &= -f\mathbf{k} \times \mathbf{u} + \alpha g \nabla \psi_e \end{aligned} \tag{3}$$

where  $\mathbf{k}$  is the unit vector (positive upward).

The transport equations of the scalars write as

$$\frac{dS}{Dt} = \frac{\partial}{\partial z} \left( \kappa \frac{\partial S}{\partial z} \right) + F_s \tag{4}$$

for salt

$$\frac{dT}{Dt} = \frac{\partial}{\partial z} \left( \kappa \frac{\partial T}{\partial z} \right) + \frac{\dot{Q}}{\rho_0 C_p} + F_h, \tag{5}$$

and temperature.

The above system of equations is closed with the equation of state, the definition of the tidal potential and Coriolis factor and the parameterisation for horizontal and vertical mixing derived from turbulence closure equations. For the latter, SCHISM uses the generic length scale (GLS) formulation of Umlauf and Burchard (2003) to solve for the

transport, production and dissipation of the turbulent kinetic energy, and in this paper the k-kl scheme is used. Velocities in the bottom boundary layer follow the logarithmic law. The bottom stress

$$\tau_b = C_D |\mathbf{u}_b| \mathbf{u}_b \tag{6}$$

is formulated for a turbulent boundary layer, in which  $\mathbf{u}_b$  is the horizontal bottom boundary velocity and the drag coefficient  $C_D$  is given by

$$C_D = \left( \frac{1}{k_0} \log \frac{\delta_b}{z_0} \right)^{-2} \tag{7}$$

with  $k_0$  := the von Karman constant,  $\delta_b$  := the thickness of the bottom cell and  $z_0$  being the bottom roughness.

### 3.1.2 The numerical formulation

SCHISM uses unstructured triangular-quadrangular grids in the horizontal direction (see the inset in Fig. 1c) and hybrid SZ or LSC<sup>2</sup> (Zhang et al. 2015a) coordinates in the vertical. The domain is discretised horizontally with 363,448 nodes, which are connected in a network of 715,254 triangles. For simplicity, the vertical discretisation uses a pure S coordinate formulation with 41 layers and more resolution skewed towards the free surface. The horizontal resolution varies from a coarser resolution of 700 m at the domain boundaries to a finer resolution for the Wadden Sea, where the bathymetric channels are resolved with a resolution of about 200 m (Fig. 1c). The unstructured grid was created using the Surface-water Modeling Software, SMS from Aquaveo (<http://www.aquaveo.com/>).

The system of equations is solved by SCHISM using finite-element and finite-volume schemes. The applied schemes are semi-implicit for all equations to by-pass mode splitting (into external and internal modes) and thus the associated splitting errors. The terms of the barotropic-pressure gradient, the vertical viscosity in the momentum equations and the divergence term in the continuity equation are treated implicitly ([http://ccrm.vims.edu/schism/combined\\_theory\\_manual.pdf](http://ccrm.vims.edu/schism/combined_theory_manual.pdf)).

The continuity and momentum equations are solved simultaneously and are decoupled via the bottom boundary layer (Zhang and Baptista 2008). The momentum advection is treated with an Eulerian-Lagrangian method (ELM) to further enhance stability. For the current simulations, a time step of 120 s was used resulting in Courant-Friedrichs-Lewy (CFL) numbers  $> 0.4$  used as orientation to avoid excessive truncation errors in the ELM (Zhang et al. 2015a).

An important feature, which makes SCHISM suitable for the area of interest, is its capability to simulate wetting and drying in shallow areas such as the Wadden Sea. A node is marked as wet (or dry), when the total depth  $H$  at the

node exceeds (or falls below) a specified minimum depth  $h_0$ , which was set as 1 cm in this study.

### 3.2 Numerical experiments

#### 3.2.1 Initialisation and forcing

The model was initialised with a “hotstart” state, which was generated by integrating the model for 1 month starting from a climatology dataset (Janssen et al. 1999). The period of 1 month appeared long enough for the shallow areas considered here to reach a quasi-equilibrium state.

At the open boundaries, the model is forced by timeseries of sea-surface elevation, salinity, temperature and velocity. Those variables were derived from hourly values from the outputs of the North-West European Continental Shelf (NWS) operational model (O’Dea et al. 2012) and interpolated onto the boundary grid nodes at the model time step of 120 s. Atmospheric forcing (wind, atmospheric pressure, air temperature and specific humidity) was taken from the operational atmospheric model of the German Weather Service’s (Deutscher Wetter Dienst, DWD) COSMO-EU. River runoff data in the region are provided by the BSH.

#### 3.2.2 Design of experiments and their nomenclature

The only difference in the three sensitivity experiments presented below is in the bathymetries used: BR-Experiment (BRE); B2000-Experiment (B2000E) and B2011-Experiment (B2011E). The three experiments were performed without active morphodynamics, i.e. the bathymetry did not change, but just represented different states: the BR in BRE, B2000 in B2000E and B2011 in B2011E, respectively.

We recall that the bathymetries used are compiled using inputs that are identical for most of the model area and differ only in its south-eastern corner. Because similar data are not available for the entire southern North Sea, the results of experiments with different topographies available to us cannot fully reveal the change of circulation in the southern North Sea during the last decades caused by the basin-wide bathymetry change. Therefore, a decision was taken to focus on the sensitivity of numerical model to realistic bottom changes in one region only while keeping the forcing the same in all experiments; the period of analysis is 07/02/2011 to 07/16/2011. An alternative approach using topographic noise in the whole model area in order to study the response to changes (or errors) in bathymetry has been recently proposed by Schulz-Stellenfleth and Stanev (2015). The sensitivity experiments described below make one concrete step forward in addressing the sensitivity of the entire southern North Sea to different bottom topographies in one

region. Theoretically, our experiments can also be interpreted as analysis of a model with topographies of different quality (experiments with time-referenced data compared to experiments using BR). The better solution would be to have time-slices of bathymetry based on homogeneous observations in the entire basin, but such data with very fine resolution will unlikely be available in the coming years.

The modelling strategy adopted here has something in common with the ocean downscaling. This approach assumes that regional models are forced with data simulated by models covering larger areas (usually with coarser resolution), but resolve local conditions better and give new details of ocean state in the nested domain. In the experiments presented in the following, the time-referenced bathymetry in the coastal part of southern North Sea is supposed to better resolve local conditions in comparison to bathymetries using all data available in a region. Furthermore, with an unstructured-grid model, we avoid using multiple nests in the coastal ocean (e.g. Stanev et al. 2014).

In addition to downscaling, our simulations and the analyses presented in the following are also aimed at demonstrating upscaling aspects (Schulz-Stellenfleth and Stanev 2015). In general, upscaling can be regarded as a process in which information is transferred from a smaller scale to a larger scale. However, as it has been made clear by those authors, possible inconsistency between observations taken in coastal areas and open boundary forcing of numerical model is a demonstration of propagation of coastal signals far from their area of origin (upscaling). Thus, like in Schulz-Stellenfleth and Stanev (2015), we will study the large-scale impact of bathymetry in coastal domain. The difference is that we address sensitivity in the southern North Sea to different time-referenced topographies.

As described in Section 2.2, the major differences between bathymetries are found in the area of the German Wadden Sea (Fig. 2a). Since the mean depth in all data sets remained almost the same, the different responses to them will reveal the role of changes in the macro roughness. Simulation results from BRE will be analysed in the following to illustrate the hydrodynamics of the study area. B2000E and B2011E will illustrate the changes in hydrodynamics resulting from using time-referenced topographies. The comparison between the results of three sensitivity experiments presented below will help answer the question: how important is the change of small-scale topographic roughness on the regional and larger-scale dynamics?

### 3.3 Model performance

#### 3.3.1 Validation against earlier concepts

In the following model, results from the experiment with the reference bathymetry (BR) for one neap-spring period from



07/02/2011 to 07/16/2011 will be analysed. The simulated sea level is first subject to harmonic analysis performing a least square fit with a set of eight constituents.

Other variables are not analysed here because elevation is a good indicator for responses addressed in the present study as it integrates all volume fluxes, including density driven flows. Here, we refer to the paper of Zhang et al. (2015c) for more details about validation of thermohaline fields simulated with SCHISM in the area of North Sea.

The dominant tidal constituents were estimated from simulations using harmonic analysis (Pawlowicz et al. 2002). Figure 5a demonstrates that the dominant M2 constituent rotates in a counterclockwise direction around three amphidromic points (AP). These are located at (1)  $-1.77^{\circ}\text{E}$ ,  $50.61^{\circ}\text{N}$ , which is in the English Channel at the southern coast of Great Britain, (2)  $2.81^{\circ}\text{E}$ ,  $52.36^{\circ}\text{N}$ , which is in the center of the Southern Bight and (3)  $5.27^{\circ}\text{E}$ ,  $55.27^{\circ}\text{N}$ , which is in the central southern North Sea. The shape of co-tidal lines drawn with intervals of  $30^{\circ}$  are consistent with what is known from earlier analyses in the North Sea since the pioneer review of Proudman and Doodson (1924). The English Channel is also the region where the largest amplitudes within the domain are reached with maximum values of  $\sim 5$  m in the southeastern-most bight of the Channel (Fig. 5a). Within the English Channel, the amplitudes of M2 tide and the shape of phase lines are in good agreement with the results of Walters (1987). Another zone of local maximum M2 amplitudes of  $\sim 2$ – $2.5$  m near The Wash also agrees with previously known tidal characteristics in the southern North Sea.

It is known that in the tidal basins 2D models represent qualitatively well the basic properties of tidal wave. One could then expect that for the aims of present study it would be sufficient to use a 2D model. In order to check this, the reference 3D run was repeated with SCHISM in 2D mode. Manning roughness coefficient was specified as 0.025 (Manning et al. 1890). The differences between the simulations presented in Fig. 5b as root mean square difference (RMSD) between outputs from the two runs demonstrate clearly that the largest differences appear in the embayments along the eastern coast and in the English Channel. In the deep parts of model area, the 2D model is pretty accurate. These results illustrate that in the shallow coastal areas, where the role of friction is large and where baroclinicity can also be important because of river runoff, the 2D simulations can be strongly biased. The largest RMSD in the eastern part of model area exceeds 0.5 m (Elbe and Weser estuaries and Jade Bay). Even larger are the differences in some other areas where fresh water fluxes are minor, which demonstrates that a fundamental problem with the 2D model is to adequately represent the friction in coastal areas. Because we focus on the Wadden Sea, where drawbacks of 2D model are quite significant (i.e. water

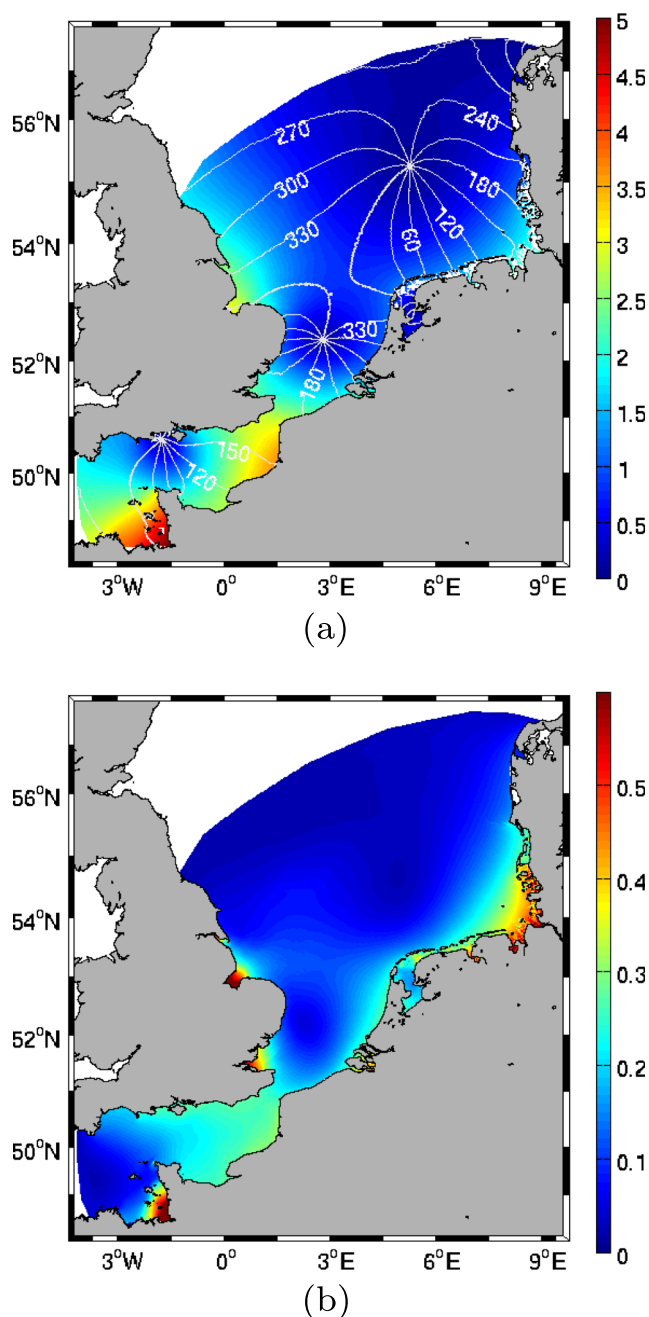
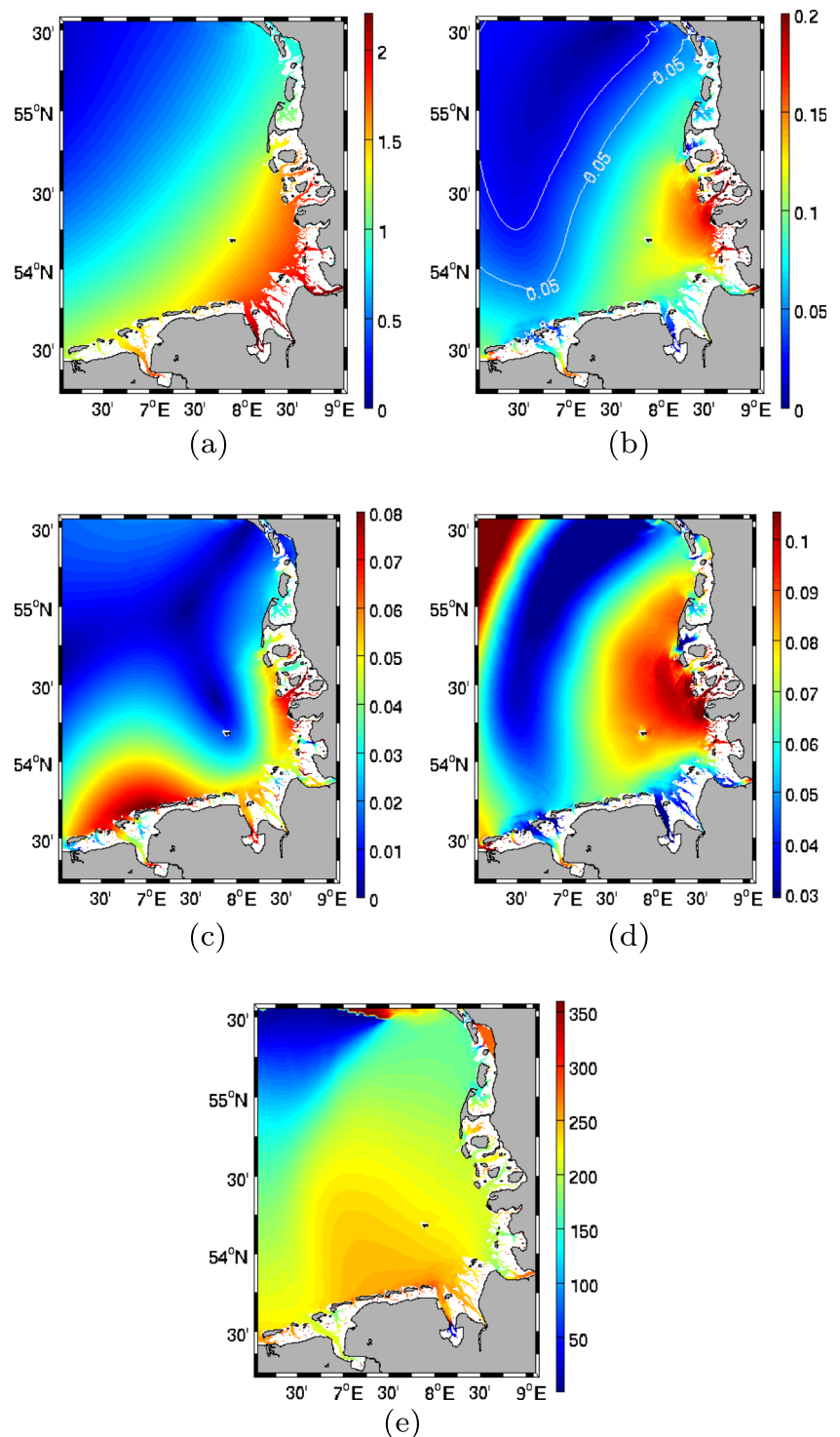


**Fig. 5** **a** Tidal amplitudes (color coded in m) and phase lines (white, in  $^{\circ}$ ) of the M2 constituent in the southern North Sea based on the data from simulations with 3D reference run (BRE). **b** Root mean square difference (RMSD) of sea surface elevation (in m) between the 3D reference run and 2D simulations. The RMSD is large in the shallow coastal areas, where the role of friction is also large and baroclinicity can be important

level difference in two runs approaches the half of the tidal amplitude (Fig. 5b), the use of the 3D model gives more realism.

In the German Bight, the amplitude of M2 tide (Fig. 6a) shows an increase from the AP towards the coast, reaching

**Fig. 6** M2 (a), M4(b) and M6(c) tidal amplitudes (in m) estimated from the reference run (BRE) in the German Bight. In (b), 0.025 m and 0.05 m isolines are also plotted. Tidal asymmetry is illustrated by the ratio in M4 and M2 amplitude (d) and the according phase difference  $\phi_{M4} - 2\phi_{M2}$  (e). Here, and in other similar figures, *white areas* are where tidal analysis could be biased because these zones fall dry



a maximum in the area of Elbe and Weser River mouths. Along the southern coast, the amplitude increases from  $\sim 1$  m in front of the West Frisian Wadden Sea to  $\sim 2$  m in the narrow channels of Jade, Weser and Elbe (Fig. 6a). The reflection and refraction of Kelvin waves in the coastal regions of German Bight are accompanied by a pronounced distortion of the tide, thus enhancing the over-tides. The

numerical simulations support similar results known from structured-grid modelling (Stanev et al. 2014), revealing an amplification of the M4 constituent in front of the North Frisian Wadden Sea (Fig. 6b). Because tidal analysis could be biased on the tidal flats, which fall dry during part of tidal cycle, some coastal regions are excluded from the analysis (white areas in Fig. 6).

The minimum in the M4 amplitude extends from the westernmost tip of the Danish coast (see the position of Esbjerg in Fig. 1a, which is close to the position of the M4 amphidromic point) to the southwest German Bight following a curved line toward the region of the Ems Estuary (see the shape of white isolines in Fig. 6b).

The M6 tide in the German Bight (Fig. 6c) shows two pronounced local maxima with amplitudes of up to 8 cm. The larger one shows a half-circle pattern in front of the East Frisian Wadden Sea with its centre in front of Juist Island. Behind the islands protecting the region of Ems Estuary, the M6 amplitude reduces strongly landwards along the tidal channels. However, the relatively wider Jade Channel provides a better pathway of propagation of M6 tide in the direction of Jade Bay. The second pronounced maximum of M6 is located in the southern part of North Frisian Wadden Sea and coincides with the region of maximum M4 tide, and thus both nonlinearity and friction are very important there.

The strength of tidal asymmetry measured as the ratio between M4 and M2 amplitudes (Fig. 6d) shows similarity with the pattern of M4 amplitude, thus mirroring the regions of maximum and minimum M4 amplitudes. The dubious maximum of this ratio in the northwestern corner of German Bight is explained by the proximity of amphidromic point of M2 tide (see Fig. 5a). The maximum M4/M2 ratio is up to 10 % south of Sylt.

Tidal asymmetries can be identified in many ways: by comparing the maximum flood and ebb velocities, by estimating the difference in the duration of the flood and ebb tidal phases or by analysing the transport of suspended matter. One example of the characteristics of tidal asymmetries in the Wadden Sea has been given by Stanev et al. (2003). In this example, the relevance of dominant balances in this area to dynamics of tidal estuaries was made clear. In another example of Stanev et al. (2014), tidal asymmetries are studied for a much larger area, which is the German Bight.

The analyses presented here are similar to the ones cited above, but are based on the phase difference  $\phi_{M4} - 2\phi_{M2}$  as an independent measure of tidal distortion. Applying this difference to signals of sea surface elevation (Fig. 6e), values between  $0^\circ$  and  $180^\circ$  denote ebb dominance (rising tide exceeds falling tide in duration) and values between  $180^\circ$  and  $360^\circ$  denote flood dominance. For more detail about identifying flood/ebb dominance via the phase difference between M2 and M4, we refer to Speer (1984).

As seen in Fig. 6e over most of the German Bight, tidal asymmetry is between  $180^\circ$  and  $360^\circ$  indicating flood dominance, in particular in front of the East Frisian Wadden Sea. Sharp transition of asymmetry from flood to ebb dominated is observed in the Jade Bay and also in part of the Elbe Estuary.

### 3.3.2 Validation against gauge data

As demonstrated in the previous section, the overall shape of co-tidal and amplitude lines agrees well with the results from previous modelling work. The correlation between simulations and observations demonstrates that tidal characteristics in coastal locations are also of good quality. Because an extensive intercomparison of the model against observations is presented in Zhang et al. (2015c), we will keep the validation against observed data here short.

Data used to validate the model from tide gauges were taken from the MyOcean project for the stations Whitby, Dover, Borkum and Helgoland (Blanc 2008).

The agreement between model and data is presented as a Taylor diagram (Fig. 7) that combines information on correlation, variability and root mean square error (RMSE). The correlation for the different stations ranges between 0.96 and 0.99 and shows that the model can reproduce the overall dynamic seen in the data. The scaled standard deviation reveals a slight tendency for the model to overestimate the variability.

The relative difference between observations and simulations is more pronounced in Helgoland and in the Wadden Sea (Borkum station) where the tidal amplitude is smaller than those along the western coast and in the English Channel (Fig. 8a). The phases of M2 tide (Fig. 8b) are overall in good agreement with observations revealing small phase shifts of  $\sim 5\text{--}10^\circ$  at all four stations.

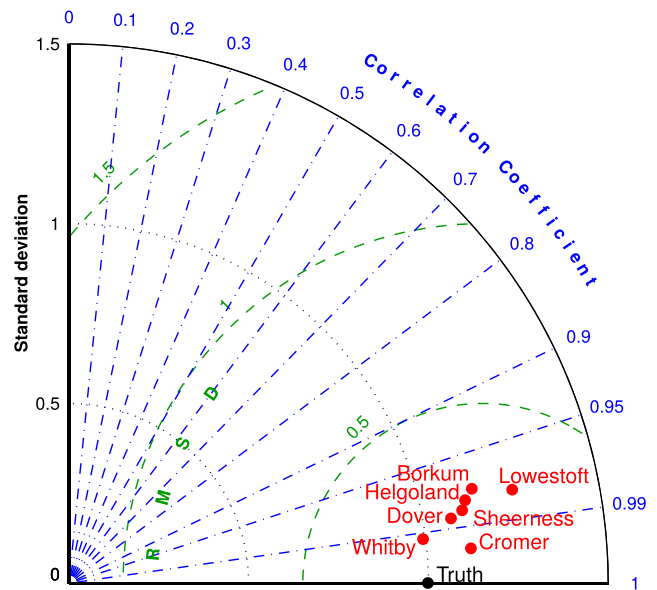


**Fig. 7** Taylor diagram, showing root mean square difference, correlation and standard deviation between the model and data from different tide gauge stations (●). The standard deviation is given as the standard deviation of the model divided by the standard deviation of the data. The hypothetical truth point (●) indicates the position of 100 % agreement between data and model

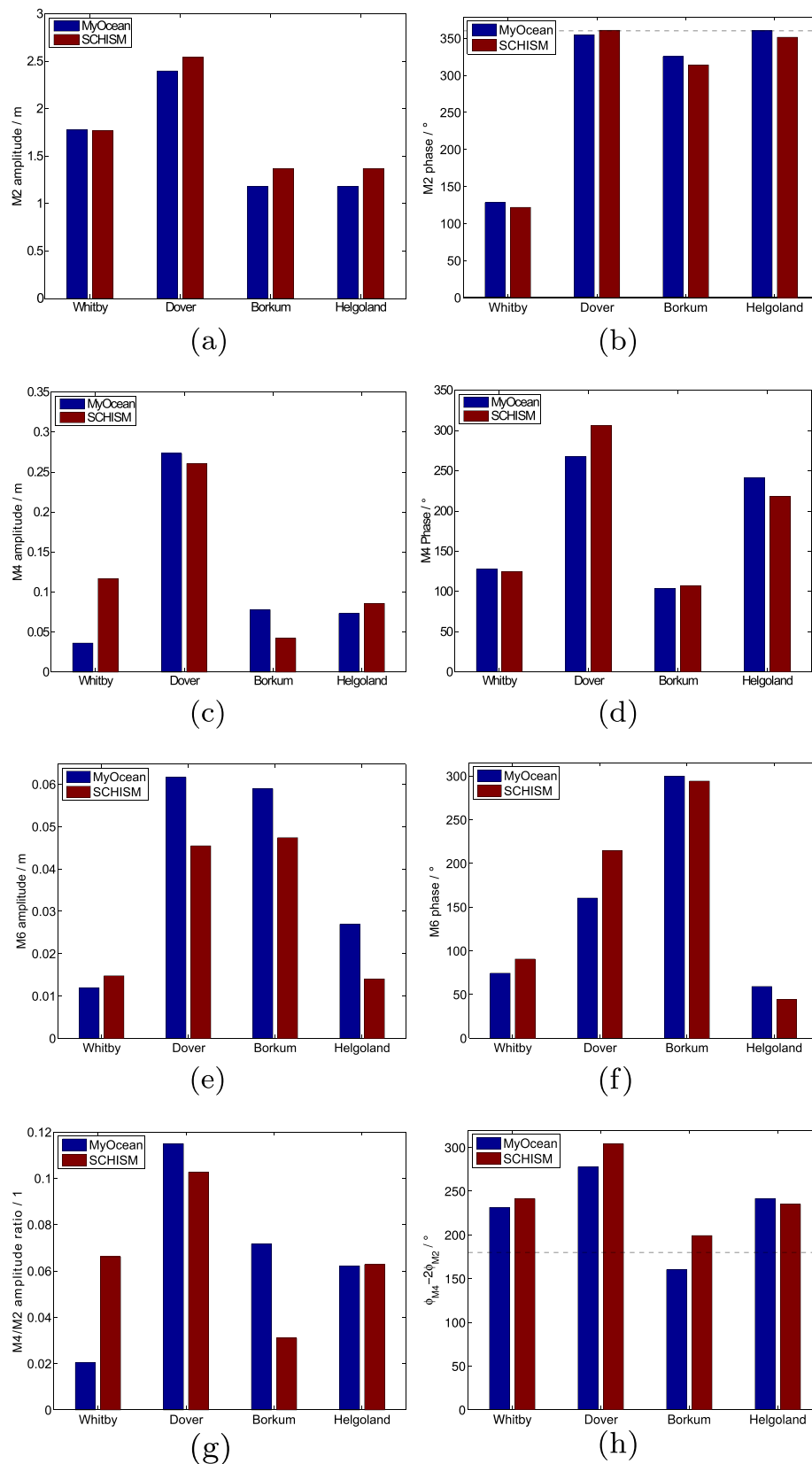


**Fig. 8** Validation of dominant tidal constituents simulated with SCHISM against MyOcean tide gauge data at selected stations. Validation of the amplitude (*left panel*) and the phase (*right panel*) are shown

for the constituents M2 (**a,b**), M4 (**c,d**) and M6 (**e, f**). Tidal asymmetry is presented as the M4:M2 ratio in (**g**) and phase shift (**h**)



The amplitude of M4 tide varies between 25 cm in Dover and less than 10 cm elsewhere. The smallness of this signal makes the correct simulation of over-tides very challenging. As seen in (Fig. 8c), the model tends to underestimate the amplitudes. One exception is in the station Whitby, where the M4 amplitude is overestimated. In the English Channel where the energy associated with the M4 tide is high, the simulations match the observations much better. The problems mentioned above could be attributed to the nonlinear distortion of tides in the coastal areas.

The amplitude of the M6 overtide which is generated by friction is lower than the amplitude of the M4 overtide (Fig. 8e). While the large values at Dover are explained by the strong currents in the shallow channel, the large values at Borkum (similar in the observations and simulations) are explained by the large-scale maximum of M6 tide in this region (see Fig. 6c). The phases from observations and simulations, like in the case of M4 tide, are in a relatively good agreement with each other (Fig. 8f).

The asymmetry which is characterised by the ratio of M4 and M2 amplitudes and  $\phi_{M4} - 2\phi_{M2}$  (Speer 1984) reveals large differences in the individual stations. The largest amplitude ratio is at Dover ( $\approx 0.12$ ) and the observations and simulations give similar values there. However, problems with the accuracy of M4 representation and its very low magnitude explain substantial differences at individual stations, as well as the differences between observations and simulations. One representative of this problem is at Whitby where M4 tide is overestimated by the model. At Helgoland station where M2 and M4 tides are similarly overestimated the amplitude ratio in observations and simulations is fortuitously close. With respect to the phase shift  $\phi_{M4} - 2\phi_{M2}$ , the agreement between observations and simulations is much better (Fig. 8h). At all stations, the relative phase differences derived from the observation are greater than 180 degree (flood dominant) with an exception at the Borkum station where the phase difference is slightly below 180 degree. The largest flood asymmetry, at  $\sim 270$  degrees is observed and simulated at Dover station. The model slightly overpredicts the shift towards flood asymmetry.

## 4 Results from the sensitivity experiments with time-referenced bathymetries

### 4.1 Local and basin wide response to morphodynamic change

The results from the three experiments are compared below for one neap-spring period from 07/02/2011 to 07/16/2011. First B2011E and B2000E are compared and the resulting differences in the constituents of M2 and M4 tide are explained.

This comparison aims at elucidating the hydrodynamic response. At the end, we compare these two experiments with BRE. The latter will reveal the possible errors when no time-referenced bathymetries are used.

The RMSD between the simulated sea levels in B2011E and B2000E is small over most of the North Sea area with a range of few millimetres only (Fig. 9a). However, what is striking in Fig. 9a is the quadrupole pattern identified by the isolines with two maxima (in the German Bight and in front of The Wash) and two minima (along the Dutch coast and along the north-western part of model boundary). This is not a trivial result because it was hard to anticipate that relatively small changes in bathymetry in one small coastal region could trigger remote changes of tidal variability. The explanation is that the sloshing modes (Maas 1998) and Kelvin Wave unify the basin-wide responses to local bathymetric changes. Thus, the tidal signals in the two opposite ends of the North Sea are strongly anti-correlated (Fig. 10). Therefore, change of local characteristics of tidal wave by virtue of small change of the bathymetry in the Wadden Sea creates a clear tidal response in the opposite part of the sea (The Wash). At the Wash, there is a clear negative correlation with the oscillations in the eastern German Bight (notice the EOF pattern and the temporal change of sea-surface elevation in Fig. 10). Not only around The Wash but also in the Bay of Thames the difference between the two experiments is more pronounced. The amplification of the responses in the two bays is explained as a result of the funnelled-like coastline supporting increase in the tidal amplitudes.

One important question is whether the results presented above are partly due to possible problems with boundary forcing or the relatively small size of the model domain. In order to answer this question, we present a second model which is used here just to validate the credibility of simulations with the model used in the present study.

This model is presented in detail by Zhang et al. (2015c). It uses the same numerical code (SCHISM) but it is setup for the North Sea and Baltic-Sea area (Fig. 11). The numerical grid consists of about 290,000 nodes and 560,000 triangular grid elements, therefore, having a lower resolution than the model for the southern North Sea. In the vertical 31 S layers are used and the computational time step is 120 s. This model uses the same atmospheric boundary conditions as in the experiments considered above. Outputs from the North-West European Continental Shelf (NWS) operational model (O’Dea et al. 2012) are used to prescribe open ocean boundary conditions at the Scottish-Norwegian boundary. The initial conditions for salinity and temperature are taken from the same climatology data set as in the present model.

Using this larger-domain model, two experiments were conducted following B2011E and B2000E. For these experiments, the time-referenced bathymetries of B2011 and

**Fig. 9** Root mean square difference (in cm) between the sea-surface elevation in B2000E and B2011E for the entire model area (**a**) and two coastal zooms (**b** and **c**). The intertidal area is blanked out. The colour bars are chosen differently in (**a–c**) in order to better visualise the regional characteristics

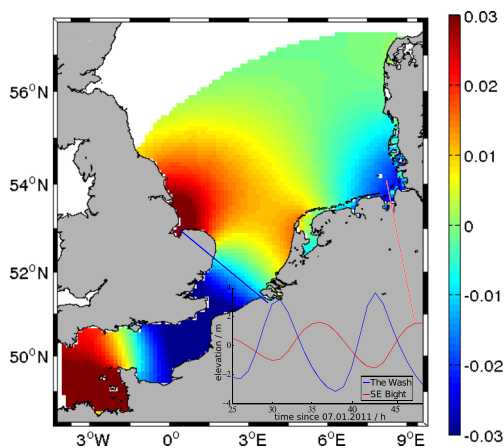
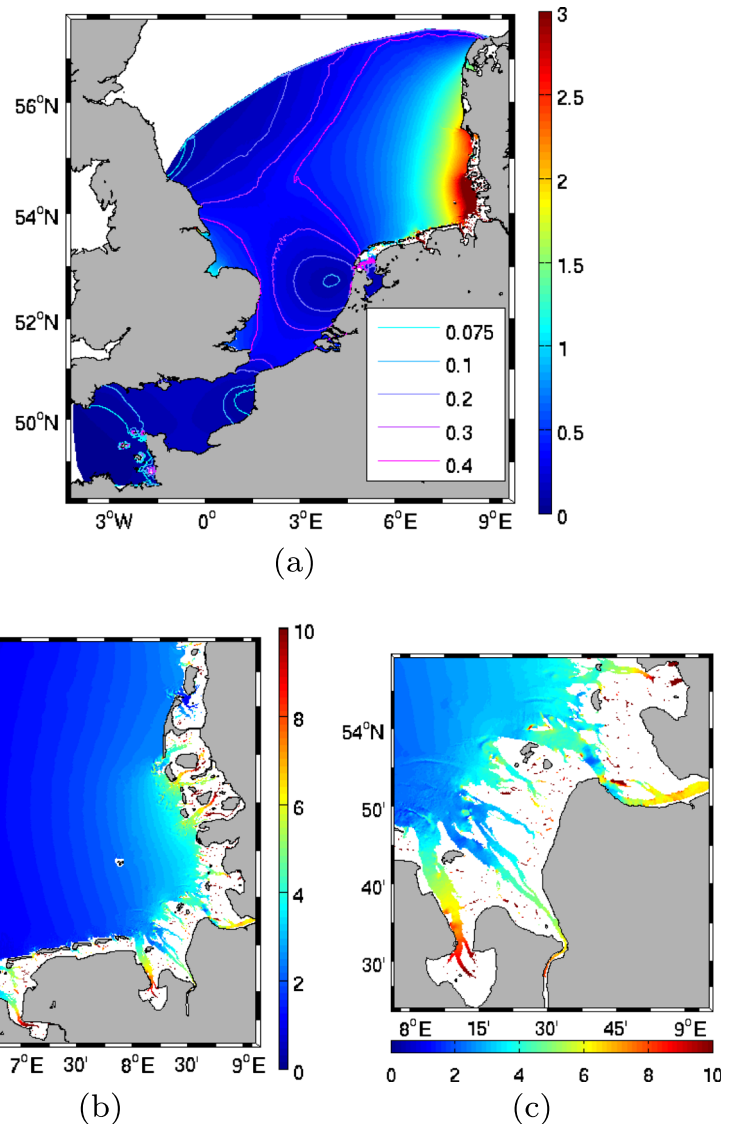


**Fig. 10** Spatial pattern of the dominant empirical orthogonal function (EOF) of sea surface elevation. The pattern shows the negative correlation between the wash and parts of the German Wadden Sea, which is further illustrated by the inset giving the temporal change of sea level in Helgoland and The Wash

B2000 were interpolated onto the grid of the larger-area model. The difference between two simulations estimated as RMSD is shown in Fig. 11 for the same period during which analysis of B2011E and B2000E has been performed. These results lend credence to the simulations carried out in the smaller domain. This eliminates possible reason that response effects in the the model of southern North Sea could be a consequence of problems with model area or boundary conditions. These results demonstrate the robustness of our conclusions presented above. The quadruple pattern seen in the simulations in southern North Sea area persists also in the bigger domain. Furthermore, tidal amplifications are also observed in other deep bays along the western coast, as in the Firth of Forth and the Morray Firth. It is interesting to note that the area with maximum differences between two simulations follows the Danish coast and can be even traced down to the Danish strait area. This

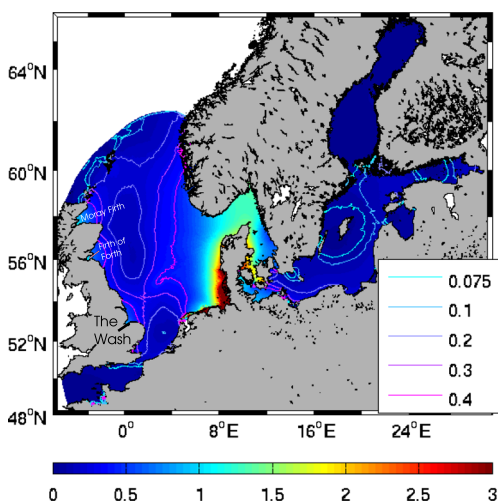


**Fig. 11** Root mean square difference (in cm) between the sea-surface elevation simulated in runs using the reference bathymetry (BRE) vs. the bathymetry of the AufMod time slice for the year 2000 (B2000E) in a larger-domain model including both the North and the Baltic Sea. The patterns being similar to those of the simulations with North Sea model ensure that the shown features are independent of the location of the domain boundary in the original experiment (Fig. 9)

propagation pattern is due to the fact that tidal wave propagates with the coast on its right; Kelvin waves in the transition area between North and Baltic Sea are analysed by Stanev et al. (2015). Obviously, this issue needs further investigation because of possible strong coupling of dynamics at both sides of the Danish Peninsula.

As expected, the largest deviations between the BRE, B2011E and B2000E were localised in the area having different bathymetries, i.e. the German Wadden Sea. Following the southern coast, the deviation between the two experiments with time-referenced bathymetry increased towards the east reaching values of more than 2 cm in front of the barrier islands (Fig. 9b).

These deviations increased further along the tidal channels reaching maximum values of up to 20 cm at the head of estuaries (Fig. 9c). An exception was the Elbe Estuary (Fig. 9c), along which the RMSD was relatively constant (~7 cm). Another non-trivial result was that the topographic changes had relatively minor impact off the East Frisian Wadden Sea, in contrast to the situation in front of the North Frisian Wadden Sea (Fig. 9b). The tendency for the impact to propagate in the direction of Kelvin wave and to localise along the eastern coast was commented above in the context of simulations in the North Sea-Baltic Sea model domain. This finding is supported by the experiments of Schulz-Stellenfleth and Stanev (2015) who, using a simpler linear 2D model, demonstrated that when the perturbations of bathymetry cover the entire North Sea the largest response is localised along the North Frisian coast.

## 4.2 The impact of morphodynamic changes on tidal constituents and asymmetries

The differences in simulations between B2011E and B2000E are in the range of few millimetres over most of the North Sea (Fig. 9). Such small values could be expected given the relatively small differences between the bathymetries B2011 and B2000.

M2 amplitude shows an overall increase in the deeper parts of the German Bight from B2000E towards B2011E (Fig. 12a), with largest values of about 2 cm being in front of Amrum (see Fig. 1 for the position). These large differences in M2 tide between two experiments are approximately where major tidal transformation occurs (Stanev et al. 2014). Landward from the chain of barrier islands the deviation between amplitudes of M2 tide simulated in the two experiments becomes negative; this negative difference increases along the tidal channels reaching -5 cm in the Elbe Estuary, which is the region with the largest differences between B2000 and B2011 (Fig. 12a). From the German Bight, the cotidal lines in B2000E (not shown here) are shifted with respect to those in B2011E with local differences of a few degrees increasing counter clockwise up to 2.5 degrees at the northern boundary, which translates to a shift of about 5 min.

The difference between M4 tides simulated in the two experiments showed an increase of the M4 amplitude in B2011E off the North Frisian barrier islands and in the adjacent tidal channels (Fig. 12b). This is approximately the area where the difference between the M2 tides was maximum. However, the decrease of difference in M2 tide between the Jade Bay and Elbe Estuary is not followed by similar decrease in M4 tide. This complex variability results in a very complex asymmetry measured as the change of ratio between changed amplitudes of M4 and M2 tide ( $(\frac{A_{M4}}{A_{M2}})_{B2011E} / (\frac{A_{M4}}{A_{M2}})_{B2000E}$ ), (Fig. 12c), or differences between their phases ( $(\phi_{M4} - 2\phi_{M2})_{B2011E} - (\phi_{M4} - 2\phi_{M2})_{B2000E}$ ), (Fig. 12d).

The change in ratio  $A_{M4}/A_{M2}$  in Fig. 12c demonstrates a split between the eastern part of German Bight and the rest. Strong response is seen in front of estuaries, which extends up to Sylt Island. This result demonstrates that changes of large-scale tidal pattern can be enhanced by complex changes in bathymetry in the near-coastal zone (compare with Fig. 2b). It is noteworthy that changes in asymmetry expressed by the M4 to M2 amplitude-ratio (Fig. 12c), reach the maximum in the region of M2 amphidromic point, which is merely due to the artifact that M2 amplitudes there are low; the amphidromic point moves slightly in different experiments.

The large-scale pattern of the changed ratio in  $A_{M4}/A_{M2}$  between two experiments can be approximately explained as a result of the specific M4 amplitude-pattern

**Fig. 12** Differences in amplitudes of M2 (a) and M4 (b) (in cm) between the sea surface elevation simulated in the runs using the AufMod bathymetry for the year 2011 (B2011E) and 2000 (B2000E). c is the amplitude ratio M4:M2 in B2011E divided by the same ratio in B2000E. d illustrates the difference in phase asymmetries  $\phi_{M4} - 2\phi_{M2}$  between B2011E and B2000E in  $^{\circ}$ . Differences are positive if values of B2011 exceed those of B2000

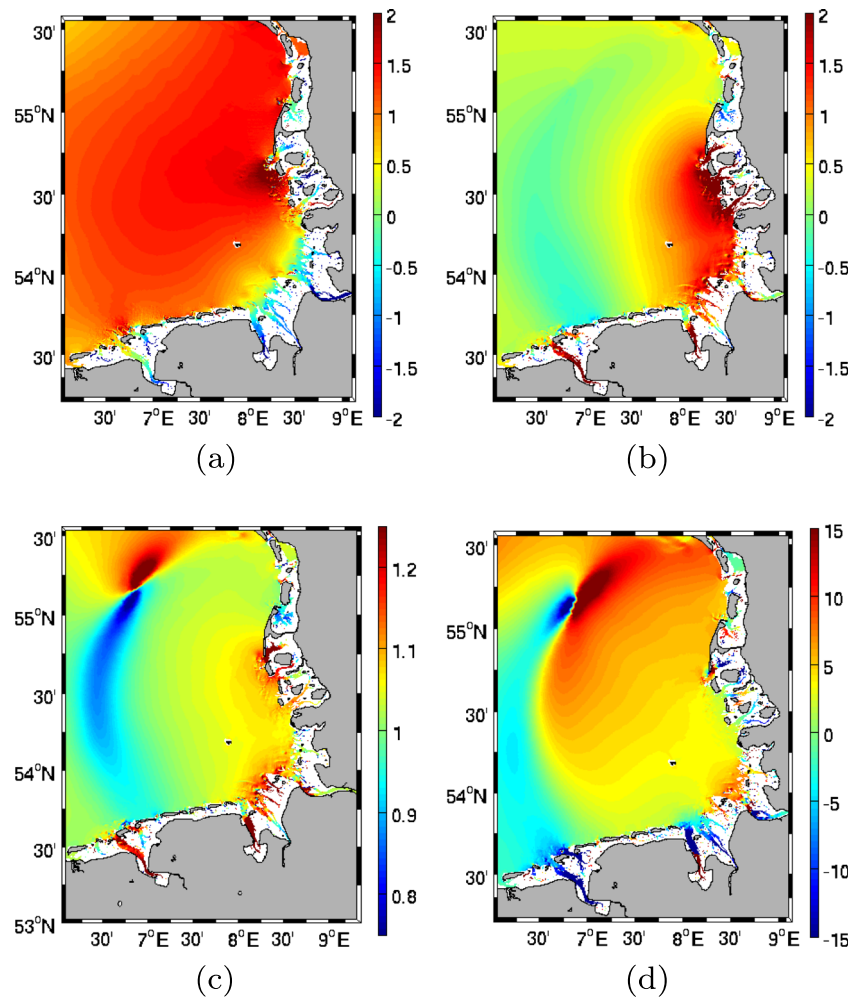


(Fig. 6b) or the ratio  $A_{M4}/A_{M2}$  shown in Fig. 6d. The changes between two experiments are large in estuaries;  $(\frac{A_{M4}}{A_{M2}})_{B2011E}/(\frac{A_{M4}}{A_{M2}})_{B2000E}$  reaching +20 % in the Ems Estuary and more than +25 % in the Jade channel.

Interesting and non-trivial response is observed in the difference between asymmetries as estimated by the phase difference  $\phi_{M4} - 2\phi_{M2}$ . The arc-like pattern originating from the areas west of the Danish coast (approximately in the area of the amphidromic point of M4 tide; where its amplitude is lowest) becomes very pronounced in Fig. 12d. It is noteworthy that this change is very unstable in different simulations, because the amphidromic point of M4 tide can easily change its position due to changes in the coastal bathymetry. The response to changed bathymetry as estimated by the change of  $\phi_{M4} - 2\phi_{M2}$  between the two experiments shows largest changes in the areas of estuaries. Flood dominance weakens in the Ems Estuary. Changes in the Jade Bay show opposite trends in its southern and northern part. In the northern part, flood asymmetry changed into ebb asymmetry. The response of the Weser Estuary to topographic change is relatively small, demonstrating a

weakening of the flood dominance by a few degrees. The most interesting changes appear in the Elbe Estuary where the above phase difference could reach  $-15^{\circ}$  in the bifurcated part of the channel; this value decreases further into the estuary. Of utmost importance for the Elbe River mouth are the opposing trends in the mouth and in the tidal river east of Cuxhaven.

To summarise, the absolute differences in the M4 tide between B2011E and B2000E (Fig. 12b) are of comparable magnitude to those of the M2 tide (Fig. 12a). Along the transition zone from deeper to shallow waters between Jade and Ems estuarine, region differences for M4 are even larger. This is also the case along the Ems Estuary and the tidal inlets in the North Frisian Wadden sea south of Sylt. Considering that the amplitude of M4 tide is about one order of magnitude smaller than that of M2 tide, changes of M4 tide in relative terms are even more remarkable.

Thus, the strong response of M4 tide to small bottom change manifests the role of nonlinear advection terms; the later are responsible for the generation of even harmonic over-tides (M4). This happens in the same area where the



refraction of tidal waves occurs, i.e. in the area of transition from eastward to northward propagation of Kelvin wave (Stanev et al. 2014). Comparisons between simulations with other time-referenced bathymetries demonstrate large diversity in the local responses, as estimated from the tidal constituents or asymmetry of tide.

#### 4.3 Experiments with time-referenced and non-time-referenced bathymetry and the effect of macro roughness

The analysis of bathymetries presented in Section 2.2 demonstrated that the difference between B2000 and B2011 is in the range of mean natural-variability estimated for the period 1983–2011. Therefore, we could consider B2000E and B2011E as two representative members of possible large number of natural states. Because time-referenced coastal data set with high resolution is not available over the entire model area, it is not possible to address in a realistic way basin-wide responses to basin-wide morphological change. This is partially the reason why we did not analyse the multitude of experiments with different (regional) bathymetries. Rather we address two specific questions: (1) how large are the differences between simulations using time-referenced and non-time-referenced bathymetries and (2) how does effect of macro-roughness compare against effect of change in the mean depth. The first question is of practical relevance because most of numerical simulations use bathymetries that present compilations of as many observations taken over long time as possible.

The above questions will be addressed using the following set of experiments. We prepare modified bathymetry B2000C (C for corrected), which has the same average depth as BR but the topographic structure in the two data sets (e.g. location of channels, deltas and sandbanks) differs. Thus, the difference between two bathymetries gives a proxy of different roughnesses used in BRE and the new experiment B2000CE (which uses B2000C). Then the difference between BRE and B2000E will help answering question (1); the difference between B2000CE and BRE will help answering question (2).

The RMSD between simulations BRE and B2000E (not shown here) is qualitatively similar to the RMSD between simulations B2011E and B2000E (Fig. 9). This gives an estimate of the possible errors caused by using non-time-referenced bathymetries (see Section 4.2 for the ranges). These errors cover large parts of the eastern German Bight and could reach 10–15 cm in the Wadden Sea and estuaries.

As the bathymetries used in BRE and B2000E differ in both average depth as well as in macro roughness, the resulting RMSD between these two experiments is expected to be larger than the difference between experiments which differ by only one of these characteristics (e.g.

BRE vs. B2000CE). Summing up the RMSD of sea levels between BRE and B2000E over all grid nodes gives a total of around 5207 cm. This is about 190 cm larger than the integrated RMSD of 5016 cm between BRE and B2000CE. This suggests that the difference in roughness is the dominant contributor for the simulated differences. Therefore, the spatial structure and magnitudes of the RMSD(BRE,B2000CE) (not shown here) are almost identical to the RMSD(BRE,B2000E).

In contrast, the sum of RMSD between experiments with the same roughness (B2000CE and B2000E) is only 383 cm, which is an order of magnitude smaller than in the case BRE - B2000C. However, the spatial pattern (not shown) is very similar to the one in Fig. 9, suggesting that the same physical mechanisms control the response to changes in the mean depth. In conclusion, the roughness effects, rather than the average depth, dominate the simulated differences.

## 5 Discussion

The unstructured-grid model used in the present study reproduces successfully the tidal dynamics of the southern North Sea. The validation against observations showed some differences in the magnitude and phase of tidal wave, which can motivate further improvement of model calibration. For the present study, which is not oriented towards operational applications, but towards sensitivity analyses, it is more important that the major processes are present in the model, allowing to address possible dynamical consequences of changes in coastal bathymetry.

Because the mean depths of BR and B2000 differ, a reasonable question was asked of whether the sensitivity to different bathymetries in the two experiments was due to the difference in mean depth or small-scale bottom features (considered as macro-roughness elements in Fig. 2). The B2000CE gave an answer to this question: the difference between the results from B2000E and B2000CE was less than 10 % of that between BRE and B2000E. This demonstrates the dominant role of macro-bottom roughness in the considered experiments. However, the spatial patterns of sea-level change caused by the changes in macro bottom roughness and mean depth in the coastal area appeared similar. The two factors enhanced friction in the Wadden Sea more in B2000E than in BRE and the travelling wave decelerated.

In order to analyse the impact of more realistic changes in bathymetry, a run resembling the bathymetry of 2011 (B2011E) was compared with B2000E. Changes in the roughness pattern were shown to influence the tidal wave propagation, which manifested in changes of the tidal constituents.

The relative changes in the M4 tide caused by changing bathymetry of Wadden Sea appeared higher compared to those seen in the response of M2 tide. It has also been demonstrated that these responses were primarily due to the small-scale changes in bathymetry. As the nonlinear advection terms are responsible for the generation of even harmonic over-tides (M4), the nonlinear dynamics are strongly dependent on small-scale bottom properties. Because (1) the ratio between amplitudes of M4 and M2 tides quantifies the asymmetry of tides and (2) the tidal asymmetry controls the sediment transport (Friedrichs and Aubrey 1988), the results here suggest that morphological changes (e.g. on a decadal scale) could affect the net transport of sediments. Because this process could trigger complex feedback, further analyses using models with active morphodynamics are needed.

Although the differences between the results of sensitivity experiments indicated largest values directly in the region of bathymetric change, it has to be emphasised that they were by no means limited to this region, but covered larger areas. The pattern of the differences of tides in the sensitivity experiments followed the direction of Kelvin wave propagation, demonstrating a clear tele-connectivity between remote coastal areas in the southern North Sea. The first EOF of sea level presented in Fig. 10 demonstrates clearly this tele-connectivity. The temporal variability of sea level in Helgoland and The Wash (also shown in this figure) indicates that the sloshing mode, i.e. the free-surface oscillation of a fluid in a semi-enclosed basin, provides the basis for tele-connectivity between eastern and western coasts.

The basin-scale tele-connectivity shown here could be considered as an illustration that the entire morphodynamic system of North Sea could undergo coherent changes shaped by the basin modes and Kelvin wave propagation. Similar responses could occur as a result of changes in other controlling parameters (e.g. atmospheric forcing, river runoff, etc.), which will be the subject of future study.

The large-scale responses appeared useful to elucidate the physical mechanisms, although they have very small amplitudes and cannot be easily measured. The maximum RMSD of a few centimetres in front of barrier islands are also relatively small and could lie below the error range shown in the validation (Fig. 8). However at the coastal stations and estuaries the differences in tides caused by morphodynamic changes could be measurable. What is remarkable here is that these responses (relative changes in M4 amplitude) were generated by extremely small changes in bathymetry. This makes it challenging to demonstrate that changes in bathymetry could explain long-term changes in time series from tide gauges. One useful result from the analyses shown above is that the *relative* changes in observed tidal constituents could perhaps indicate response to changing bathymetry.

With respect to the considerations presented above one has to keep in mind that the seasonal variability of tides in the North Sea is relatively strong. Gräwe et al. (2014) found for the station Cuxhaven a seasonal variability of 8–10 % for the M2 tide and 12–30 % for the M4 tide, which they attributed to the stratification in the central North Seas and its breakdown in autumn. Although seasonal changes reported by (Gräwe et al. 2014) seem to have larger contribution, one cannot exclude that changes in bathymetry may also contribute to the overall tidal variability in the studied area.

We did not address in this paper the tidal change which could be a consequence of long-term sea-level rise. We will present therefore only a preliminary characterisation of tide gauge data in coastal and open ocean stations for about one decade as a step in this direction.

From the analysis presented in Section 2.3, it became clear that the ratio between amplitudes of M4 and M2 tides is about two times larger in the coastal (Cuxhaven) than in the open-ocean (Helgoland) stations. At Borkum station, this factor is about four. This difference between open-ocean and coastal stations is consistent with a similar trend caused by bathymetric change (Fig. 12) demonstrating the larger sensitivity of M4 tide in coastal zone to changes in different elements of hydrodynamic system (atmospheric forcing or bathymetric changes). In contrast, the relative change of the M2 tide is comparable at both stations, being slightly higher at Helgoland. This result suggests that stronger signals associated with possible response to bathymetric change could be found in the coastal stations. However, the signal to noise level is small, which necessitates using more advanced analysis techniques and longer time series. Furthermore, there is a recent trend of increasing amplitude of M2 and M4 tides by few percent following an initial decrease from 2006 to 2007. This might be related to climatic changes but might also be influenced by morphodynamic process. However, analysis done so far does not show a clear trend for the ratio of M2/M4, which would otherwise identify a shift in the energy transfer to higher harmonics, and be indicative for such changes like the ones reported in the present study.

## 6 Conclusions

In this paper, we demonstrated possible regional and basin-wide responses to the changes of bottom bathymetry in the Wadden Sea caused by the migration of tidal channels. The small-scale bathymetry changes justified the use of very fine model and bathymetric resolutions. We found that small changes in bathymetry, or more precisely, changes in the macro roughness, led to system-wide response of tidal dynamics including tidal asymmetry. This has implications for the morphodynamics, because nonlinear feedback is

expected to be significant. One alternative approach would be to assess the response by imposing small-scale perturbations of bathymetry, bottom roughness, wind forcing, and boundary forcing in a series of perturbation experiments (Schulz-Stellenfleth and Stanev 2015).

It is often speculated that long-term change of sea-level would cause barrier islands to migrate while conserving mass through offshore and onshore sediment transport. This change is expected to be coupled to changes in the small-scale bathymetric features as well as to the large-scale dynamics, a topic that needs further investigation.

The results presented here suggest that the long-term changes of the North Sea morphodynamic system could be controlled by the basin-wide dynamics, which may have resulted in coherent changes in the distribution of ocean depths over large areas. Therefore, it seems advisable that studies of the long-term sea level change (e.g. Uehara et al. 2006) need to consider morphodynamics.

**Acknowledgments** We are grateful to the reviewers for their constructive and helpful comments. We acknowledge the German Federal Maritime and Hydrographic Agency (BSH), the German Weather Service (DWD), the Federal Waterways and Shipping Administration (WSV), the German Federal Institute of Hydrology (BfG) and the he partners of the AufMod project for the data made available for this study. This research is part of the initiative Earth System Knowledge Platform (ESKP) supported by the Helmholtz-Association. Part of this work was accomplished during the 3rd author's tenure as a HWK Fellow and financial support by Hanse-Wissenschaftskolleg (HWK, Germany) is gratefully acknowledged.

## References

- Blanc F (2008) Myocean information system. In: EuroGOOS conference proceedings
- Dronkers J (1986) Tidal asymmetry and estuarine morphology. *Neth J Sea Res* 20(2):117–131
- Dronkers JJ (1964) Tidal computations in rivers and coastal waters
- Ezer T, Liu H (2010) On the dynamics and morphology of extensive tidal mudflats: integrating remote sensing data with an inundation model of Cook Inlet, Alaska. *Ocean Dyn* 60:1307–1318. doi:10.1007/s10236-010-0319-x
- Friedrichs CT, Aubrey DG (1988) Non-linear tidal distortion in shallow well-mixed estuaries: a synthesis. *Estuar Coast Shelf Sci* 27(5):521–545
- Garcia ID, El Serafy G, Heemink A, Schuttelaars H (2013) Towards a data assimilation system for morphodynamic modeling: bathymetric data assimilation for wave property estimation. *Ocean Dyn* 63(5):489–505
- Gräwe U, Burchard H, Müller M, Schuttelaars HM (2014) Seasonal variability in M2 and M4 tidal constituents and its implications for the coastal residual sediment transport 41. doi:10.1002/2014GL060517
- Grohmann C, Smith M, Riccomini C (2009) Surface roughness of topography: a multi-scale analysis of landform elements in mid-land valley, Scotland. *Proc Geomorphom* 2009:140–148
- Heemink AW, Mouthaan EEA, Roest MRT, Vollebregt EAH, Robaczewska KB, Verlaan M (2002) Inverse 3D shallow water flow modelling of the continental shelf. *Cont Shelf Res* 22:465–484. doi:10.1016/S0278-4343(01)00071-1
- Heyer H, Schrottko K (2013) Aufbau von integrierten modellsystemen zur analyse der langfristigen morphodynamik in der deutschen bucht-aufmod
- Hirose N (2005) Least-squares estimation of bottom topography using horizontal velocity measurements in the Tsushima/Korea Straits. *J Oceanograp* 61:789–794. doi:10.1007/s10872-005-0085-4
- IOC, IHO, BODC (2003) Centenary edition of the gebco digital atlas, published on cd-rom on behalf of the intergovernmental oceanographic commission and the international hydrographic organization as part of the general bathymetric chart of the oceans. British oceanographic data centre, Liverpool
- Janssen F, Schrum C, Backhaus J (1999) A climatological data set of temperature and salinity for the baltic sea and the north sea. *Deutsche Hydrografische Zeitschrift* 51(9):5–245. doi:10.1007/BF02933676
- Le Provost C, Lyard F, de Midi-Pyrénées O (2003) The impact of ocean bottom morphology on the modelling of the long gravity waves, from tides and tsunami to climate. *Charting the Secret World of the Ocean Floor The Gebco Project* 1903
- Losch M, Wunsch C (2003) Bottom topography as a control variable in an ocean model. *J Atmosph Ocean Technol* 20:1685–1696. doi:10.1175/1520-0426(2003)020<1685:BTAACV>2.0.CO;2
- Maas LM (1998) On an oscillator equation for tides in almost enclosed basins of non-uniform depth. In: Dronkers J, Schefers M (eds) *Physics of estuaries and coastal seas*. Balkema, Rotterdam, pp 127–132
- Manning R, Griffith JP, Pigot T, Vernon-Harcourt LF (1890) On the flow of water in open channels and pipes
- Mourre B, De Mey P, Lyard F, Le Provost C (2004) Assimilation of sea level data over continental shelves: an ensemble method for the exploration of model errors due to uncertainties in bathymetry. *Dyn Atmosph Oceans* 38:93–121. doi:10.1016/j.dynatmoce.2004.09.001
- Mudersbach C, Wahl T, Haigh ID, Jensen J (2013) Trends in high sea levels of german north sea gauges compared to regional mean sea level changes. *Cont Shelf Res* 65:111–120
- Müller M (2012) The influence of changing stratification conditions on barotropic tidal transport and its implications for seasonal and secular changes of tides. *Cont Shelf Res* 47:107–118
- O'Dea EJ, Arnold AK, Edwards KP, Furner R, Hyder P, Martin MJ, Siddorn JR, Storkey D, While J, Holt JT, Liu H (2012) An operational ocean forecast system incorporating NEMO and SST data assimilation for the tidally driven European North-West shelf. *J Oper Oceanograp* 5:3–17
- Parker BB (1991) The relative importance of the various nonlinear mechanisms in a wide range of tidal interactions (review)
- Pawlowicz R, Beardsley B, Lentz S (2002) Classical tidal harmonic analysis including error estimates in MATLAB using TDE. *Comput Geosci* 28:929–937. doi:10.1016/S0098-3004(02)00013-4
- Pingree R, Griffiths D (1979) Sand transport paths around the british isles resulting from m 2 and m 4 tidal interactions. *J Marine Biol Assoc UK* 59(02):497–513
- Proudman J, Doodson AT (1924) The principal constituent of the tides of the north sea. *Philosoph Trans Royal Soc London Series A Containing Papers Math Physl Character*:185–219
- Robins PE, Davies AG (2010) Morphological controls in sandy estuaries: the influence of tidal flats and bathymetry on sediment transport. *Ocean Dyn* 60:503–517. doi:10.1007/s10236-010-0268-4
- Schulz-Stellenfleth J, Stanev EV (2015) Analysis of the upscaling problem—a case study for the barotropic dynamics in the north sea and the german bight. *Ocean Modell* (submitted paper)

- Scott TR, Mason DC (2007) Data assimilation for a coastal area morphodynamic model: Morecambe Bay. *Coast Eng* 54:91–109. doi:[10.1016/j.coastaleng.2006.08.008](https://doi.org/10.1016/j.coastaleng.2006.08.008)
- Smith PJ, Dance SL, Baines MJ, Nichols NK, Scott TR (2009) Variational data assimilation for parameter estimation: application to a simple morphodynamic model. *Ocean Dyn* 59(5):697–708
- Speer P, Aubrey D (1985) A study of non-linear tidal propagation in shallow inlet/estuarine systems part ii: theory. *Estuar Coast Shelf Sci* 21(2):207–224
- Speer PE (1984) Tidal distortion in shallow estuaries. PhD thesis, Woods Hole Oceanographic Institution Ma
- Stanev EV, Wolff JO, Burchard H, Bolding K, Flöser G (2003) On the circulation in the East Frisian Wadden Sea: numerical modeling and data analysis. *Ocean Dyn* 53(1):27–51. doi:[10.1007/s10236-002-0022-7](https://doi.org/10.1007/s10236-002-0022-7)
- Stanev EV, Wolff JO, Brink-Spalink G (2006) On the sensitivity of the sedimentary system in the East Frisian Wadden Sea to sea-level rise and wave-induced bed shear stress. *Ocean Dyn* 56:266–283. doi:[10.1007/s10236-006-0061-6](https://doi.org/10.1007/s10236-006-0061-6)
- Stanev EV, Al-Nadhairi R, Staneva J, Schulz-Stellenfleth J, Valle-Levinson A (2014) Tidal wave transformations in the german bight. *Ocean Dyn* 64(7):951–968
- Stanev EV, Lu X, Grashorn S (2015) Physical processes in the transition zone between north sea and baltic sea. Numerical simulations and observations. *Ocean Modell* 93:56–74
- Uehara K, Scourse JD, Horsburgh KJ, Lambeck K, Purcell AP (2006) Tidal evolution of the northwest european shelf seas from the last glacial maximum to the present. *J Geophys Res Oceans* (1978–2012) 111(C9)
- Umlauf L, Burchard H (2003) Reply to: Comments on 'A generic length-scale equation for geophysical turbulence models by L. Kantha and S. Carniel. doi:[10.1357/002224003771816016](https://doi.org/10.1357/002224003771816016)
- Walters R (1987) A model for tides and currents in the english channel and southern north sea. *Adv Water Resour* 10(3):138–148. doi:[10.1016/0309-1708\(87\)90020-0](https://doi.org/10.1016/0309-1708(87)90020-0)
- Winter C (2011) Macro scale morphodynamics of the German North Sea coast. *J Coast Res*:706–710
- Zaron ED, Pradal MA, Miller PD, Blumberg AF, Georgas N, Li W, Cornuelle JM (2011) Bottom topography mapping via nonlinear data assimilation. *J Atmosph Ocean Technol* 28:1606–1623. doi:[10.1175/JTECH-D-11-00070.1](https://doi.org/10.1175/JTECH-D-11-00070.1)
- Zhang YJ, Baptista AM (2008) SELFE: a semi-implicit Eulerian-Lagrangian finite-element model for cross-scale ocean circulation. *Ocean Modell* 21:71–96. doi:[10.1016/j.ocemod.2007.11.005](https://doi.org/10.1016/j.ocemod.2007.11.005)
- Zhang YJ, Ateljevich E, Yu HC, Wu CH, Jason C (2015a) A new vertical coordinate system for a 3d unstructured-grid model. *Ocean Modell* 85:16–31
- Zhang YJ, Stanev E, Grashorn S (2015b) Seamless cross-scale modelling with schism. *Ocean Modell* (submitted)
- Zhang YJ, Stanev EV, Grashorn S (2015c) Unstructured-grid model for the North Sea and Baltic Sea: validation against observations. *Ocean Modell* (in press)